Hindawi Publishing Corporation
International Journal of Photoenergy
Volume 2012, Article ID 206534, 10 pages
doi:10.1155/2012/206534

Research Article

Visible-Light Photodegradation of Dye on Co-Doped Titania Nanotubes Prepared by Hydrothermal Synthesis

Jung-Pin Wang,[1] Hsi-Chi Yang,[2] and Chien-Te Hsieh[3]

[1] *PhD Program of Technology Management, Chung Hua University, Hsinchu 300, Taiwan*
[2] *Department of Construction Management, Chung Hua University, Hsinchu 300, Taiwan*
[3] *Department of Chemical Engineering and Materials Science, Yuan Ze Fuel Cell Center, Yuan Ze University, Taoyuan 32003, Taiwan*

Correspondence should be addressed to Chien-Te Hsieh, cthsieh@saturn.yzu.edu.tw

Received 3 May 2011; Revised 6 July 2011; Accepted 8 August 2011

Academic Editor: Jinlong Zhang

Highly porous Co-doped TiO_2 nanotubes synthesized from a hydrothermal treatment were used to photodecompose methylene blue (MB) in liquid phase under visible light irradiation. The anatase-type titania nanotubes were found to have high specific surface areas of about 289–379 m^2/g. These tubes were shown to be hollow scrolls with outer diameter of about 10–15 nm and length of several micrometers. UV absorption confirmed that Co doping makes the light absorption of nanotubes shift to visible light region. With increasing the dopant concentration, the optical band gap of nanotubes became narrower, ranging from 2.4 eV to 1.8 eV, determined by Kubelka-Munk plot. The Co-doped nanotubes exhibit not only liquid-phase adsorption ability, but also visible-light-derived photodegradation of MB in aqueous solution. The synergetic effect involves two key factors in affecting the photocatalytic activity of Co-doped titania nanotubes under fluorescent lamp, that is, high porosity and optical band gap. The merit of the present work is to provide an efficient route for preparing Co-doped TiO_2 nanotubes and to clarifying their adsorption and photocatalytic activity under fluorescent lamp.

1. Introduction

Tubular form of TiO_2 has attracted considerable research for its potential applications in organic light-emitting diodes, photocatalysts, gas sensors, and high-effect solar cells [1–6], among others. To enhance efficient photocatalytic application, it is generally recognized to increase the active surface area of TiO_2 nanostructures [1, 5]. Recently, various titania nanotubes have been synthesized by using hydrothermal treatment [2, 7–9], soft-chemical synthesis [4], and self-organization combined with electrochemical method [1, 3]. The as-prepared titania nanotube is of mesoporosity and high aspect-ratio structures with nanocrystalline walls, showing promising candidates for use in photocatalytic (e.g., de-NO_x catalyst) [5] and photoelectrochemical (e.g., electrodes of dye-sensitized solar cell) systems [10].

Hydrothermal treatment is an efficient chemical route, capable of preparing highly porous TiO_2 nanotubes. Early work has investigated the hydrothermal synthesis of crystalline titania particles to produce high-purity titania-based nanotubes with an average diameter of *ca.* 10 nm [7–9]. This ability to fabricate the TiO_2 nanotubes is expected to positively impact realistic applicability. Apart from high porosity, one of vital concerns on the photocatalytic efficiency of TiO_2 nanostructures is based on solar light conversion. Analyzed on solar light spectrum, visible light accounts for 45% of energy from the solar radiation, whereas UV light is less than 3%-4% [11]. This reflects that only 3%-4% solar light can be applied according to the band gap of anatase-type TiO_2 of 3.0–3.2 eV [3]. One possible way for improving the efficiency in visible range is to narrow band gap or split into several subgaps of TiO_2. Pioneer studies have reported doping of TiO_2 with suitable species such as metal ions such as Pt, V, Ni, Mn, Cr, or Fe [11–14], or nonmetals such as N atoms [8, 15–18]. They have been demonstrated to improve the photocatalytic reactivity toward organic molecules under visible light illumination. Recently, the Co doping into TiO_2 nanocatalysts has been confirmed to exhibit superior photodegradation capability under visible light irradiation [19, 20]. However, to our knowledge, there are few reports

on in situ doping on TiO_2 nanotubes for enhancement of visible-light photocatalytic efficiency.

It is believed that a most straightforward approach for metallic doping would be ion implantation. Although this doping technique efficiently introduces species into TiO_2 compact layers, it unfortunately accompanies the structural damage of crystallites that may strongly reduce the photon conversion efficiency [1]. Moreover, the ion implantation is often expensive based on economic viewpoint. Within the above scope, this study intends to develop a simple hydrothermal synthesis of Co-doped titania nanotubes with cobalt nitrate +NaOH aqueous solutions. TiO_2 nanotubes with various amounts of Co dopants were synthesized to examine their photocatalytic efficiencies under visible light irradiation. The as-grown TiO_2 nanotubes were also characterized by high-resolution transmission electron microscope (HR-TEM), UV absorption, N_2 physisorption, and visible-light-derived photocatalysis of methylene blue (MB). In this study, the relationship between the visible-light photocatalytic activity and the amount of Co content has been explored. The merit of the present work is to provide an efficient route for preparing highly porous TiO_2 nanotubes and to clarifying their adsorption and photocatalytic activity under fluorescent lamp.

2. Experimental Section

2.1. Preparation of Co-TiO_2 Nanotubes. Titania-based nanotubes synthesized by hydrothermal synthesis have been reported elsewhere [2, 7–9]. The TiO_2 precursor used in this study was commercial TiO_2 nanopowders (P25, Degussa AG), consisted of *ca*. 30% rutile and *ca*. 70% anatase in crystalline phase. In the nanotube preparation, 2 g of the TiO_2 powder was mixed with 100 mL of 10 M NaOH + 0.01 M $Co(NO_3)_2$ aqueous solution, followed by thermal treatment of the mixture at 135°C in a Teflon-lined autoclave for 24 hr. Here, four molar ratios of Co to Ti were set at 1, 3, 5, and 7 mol%, respectively. We subjected the precipitate from filtration to pH-value regulation by mixing it with 1 L of 0.1 N HNO_3 solutions. To obtain anatase-type titania, the pH value of the slurry was adjusted to 1.6 by HNO_3 washing [7]. The final products were obtained by the filtration with subsequent drying at 110°C overnight.

2.2. Characterization of As-Grown Nanotubes. An UV spectrometer (Varian Cary100) was applied to analyze the reflectance spectra of titania samples, ranged from 200 nm to 800 nm in wavelength. The phase identification of TiO_2 nanotubes was characterized by XRD with Cu Kα radiation using an automated X-ray diffractometer (Philip PW 1700). HR-TEM (JEOL JEM-6500F) was used for morphological observations of the Co-TiO_2 nanotubes. Specific surface areas and pore volumes of the derived nanotubes were determined by gas adsorption. An automated adsorption apparatus (Micromeritics, ASAP 2000) was employed for these measurements. Adsorption of N_2, as a probe gas, was performed at −196°C. Nitrogen surface areas and micropore volumes of the samples were determined from Brunauer-Emmett-Teller (BET) and Dubinin-Radushkevich (DR) equations, respectively. The amount of N_2 adsorbed at relative pressures near unity (P/P_0 = 0.98 in this work) has been employed to determine the total pore volume, which corresponds to the sum of the micropore and mesopore volumes. The peak pore diameter of nanotubes can be estimated according to pore size distribution, determined from Barret-Joyner-Halenda (BJH) method.

2.3. Liquid-Phase Adsorption and Photodegradation. Adsorption experiments of MB were conducted by placing a certain amount of TiO_2 adsorber and 100 cm^3 of the prepared aqueous solution into a glass-stoppered flask. The flask was put in a constant-temperature shaker bath, with a shaker speed of 100 rpm. The adsorption temperature and period employed here were 40°C and 5 hr, respectively. Preliminary experiments had shown the adsorption process attained equilibrium in 5 hr for all TiO_2 samples used in the present study.

After liquid-phase adsorption, MB photodegradation on TiO_2 nanotubes was carried out to examine the photocatalytic reactivity under visible illumination. The photocatalytic decomposition of MB solutions was characterized by an UV-visible spectrometer (Shimadzu UV-2550). Based on the Beer-Lambert law [15], the concentration of MB aqueous solution is linearly proportional to the absorbance of measured spectrum in the concentration range around 30 mg/L. The MB-adsorbed titania slurries were also illuminated at 40°C, employing a 13 W fluorescent lamp. To ensure no UV light illumination, the irradiation from the fluorescent lamp was filtered through an UV cut filter (Newport FSQ-GG 400), which allows the visible light >400 nm pass through the filter. The incident intensity of illumination from the visible light was set at 750 μW/cm^2.

3. Results and Discussion

3.1. Textural Characteristics of Co-TiO_2 Nanotubes. The as-synthesized nanotube samples were designated as Co-1-TNT, Co-3-TNT, Co-5-TNT, Co-7-TNT, respectively, according to preparation of different Co/Ti molar ratios. In Figure 1, the microstructure of Co-TiO_2 nanotubes are illustrated by HR-TEM images. As shown in Figure 1, the as-grown Co-TiO_2 nanotubes are hollow with outer diameters of *ca.* 10–15 nm, inner diameters of *ca.* 5–10 nm, and lengths of several micrometers. Both the ends are opened, which is extremely critical for their adsorption and photocatalysis capability. The as-grown Co-TiO_2 nanotubes are generally homogeneous that is, narrow tubular size distribution. It can be observed from Figure 1 that the nanotubes are scrolls (unlike carbon nanotubes), showing unequal number of walls on both of tube sides. The typical nanotube axis is roughly along the [100] direction of the anatase crystals, as illustrated in the inset of Figure 1(a).

Figure 2 shows the typical isotherms of N_2 adsorption onto the titania nanotubes with different amounts of Co dopant prepared from the hydrothermal treatment. These isotherms are found to have the hysteresis behavior within high pressure of 0.6–0.98, reflecting that the products are mainly mesoporous. The pore structures of the titania

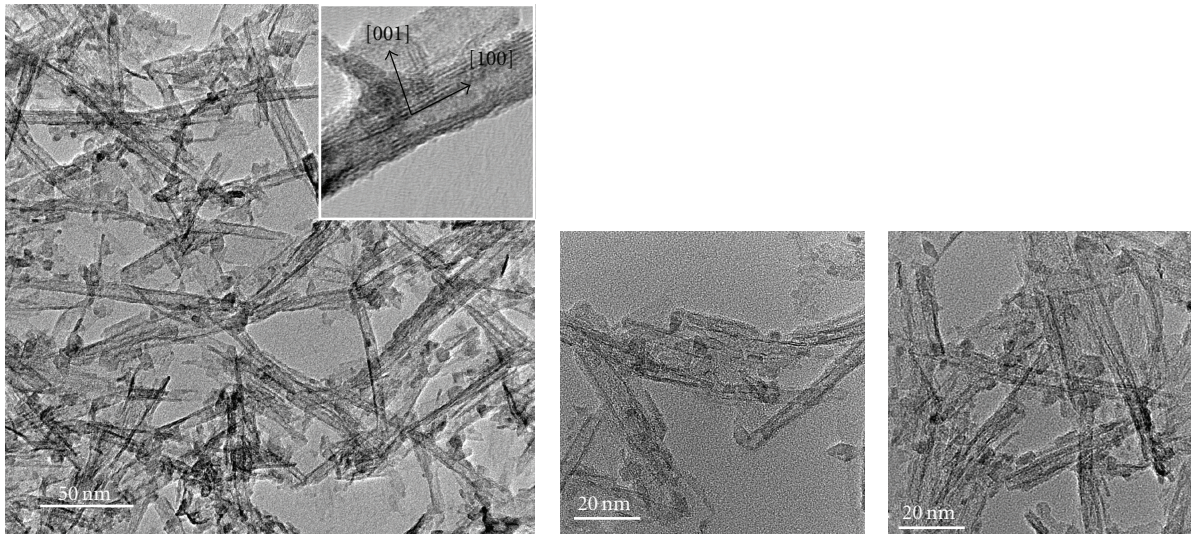

Figure 1: Typical HR-TEM image of (a) Co-1-TNT, (b) Co-3-TNT, and (c) Co-5-TNT nanotubes, prepared by the hydrothermal synthesis. The inset is the high magnification image on sidewall of the nanotube (sample: Co-1-TNT).

samples determined according to the adsorption data are also collected in Table 1. These atomic Co concentrations in titania crystallites were measured by electron diffraction spectroscopy (EDS) collected, as shown in Table 1. In comparison, the titania nanotubes (TNT) without any Co doping is used as a reference. The specific surface areas in a range of 289–379 m^2/g are much higher than for the starting material (P25), which has a surface area of *ca.* 50 m^2/g. It can be observed from this table that the titania nanotubes are highly mesoporous.

As shown in Table 1, the specific surface area is found to decrease with the doping amount. This change is probably attributed to the introduction of cobalt atoms in titania crystalline structure, thus resulting in different titania nanotubes. Indeed, this transformation of TiO_2 precursor to anatase-type titania nanotube has been well examined and reported elsewhere [2, 7]. However, the formation of Co-doped titania nanotubes prepared from hydrothermal synthesis is rarely discussed. Upon NaOH treatment, some of Ti–O–Ti bonds are broken, forming an intermediate containing Ti–O–Na, Ti–O–Co, and Ti–OH. This indicates that Co and Na atoms would occupy some broken Ti–O bonds of the TiO_2 precursor simultaneously, leading to the formation of lamellar fragments that are intermediate phase in the formation process of the nanotube material. These intermediates would proceed with rearrangement to form sheets of edge-sharing TiO_6 octahedra with Co^{2+}, Na^+, and OH^- intercalated between the sheets. Since the bond distance of Co–O is larger than that of Na–O (*ca.* 0.23 nm in NaOH) and H–O (*ca.* 0.15 nm in H_2O), the intercalation with Co^{2+} ions would result in a larger interlayer distance than that with Na^+ and H^+. Then the sheets would be scrolled to become nanotubes after HCl washing [2]. The rolling of the sheets reduces the number of surface dangling bonds, and thus lowers its system energy [8]. The presence of Co ions in these sheets would probably cause surface heterogeneity, forming different curvatures of nanotubes. This can be attributed to a fact that the Co doping affects the surface characteristics of as-grown nanotubes. The pore size distributions of these nanotubes are depicted in Figure 3, which were calculated from their N_2 adsorption isotherms, using BJH method. These distributions are found to have one, two, or three peaks in mesopore size range. The peak pore sizes range from 8 to 15 nm, identical with the HR-TEM observation. This implies that both tips of nanotubes are opened and their inner cavities are accessible to N_2 gas molecules. It can be inferred that the inner cavities in nanotubes possess a major contribution to the total pore volume.

Table 1: Surface characteristics of Co-TiO_2 nanotubes determined from N_2 physisorption at −196°C.

Materials type	C_{Co}[a] (ions/cm^3)	S_{BET}[b] (m^2/g)	V_t[c] (cm^3/g)	Pore size distribution	
				V_{micro}[d] (%)	V_{meso}[e] (%)
P25	—	45.8	0.121	0.016 (16)	0.102 (84)
TNT	0	376	0.929	0.118 (13)	0.811 (87)
Co-1-TNT	1.90×10^{20}	379	0.934	0.117 (13)	0.816 (87)
Co-3-TNT	4.31×10^{20}	350	0.975	0.118 (12)	0.857 (88)
Co-5-TNT	5.59×10^{20}	341	0.932	0.117 (12)	0.815 (88)
Co-7-TNT	7.31×10^{20}	289	0.685	0.118 (17)	0.567 (83)

[a] C_{Co}: cobalt atomic concentration determined from EDS analysis.
[b] S_{BET}: specific surface area computed using BET equation.
[c] V_t: total pore volume estimated at a relative pressure of 0.98.
[d] V_{micro}: micropore volume determined from DR equation.
[e] V_{meso}: mesopore volume determined from the subtraction of micropore volume from total pore volume.

3.2. XRD and UV Absorption of Co-TiO_2 Nanotubes. The XRD patterns of as-grown titania samples with different

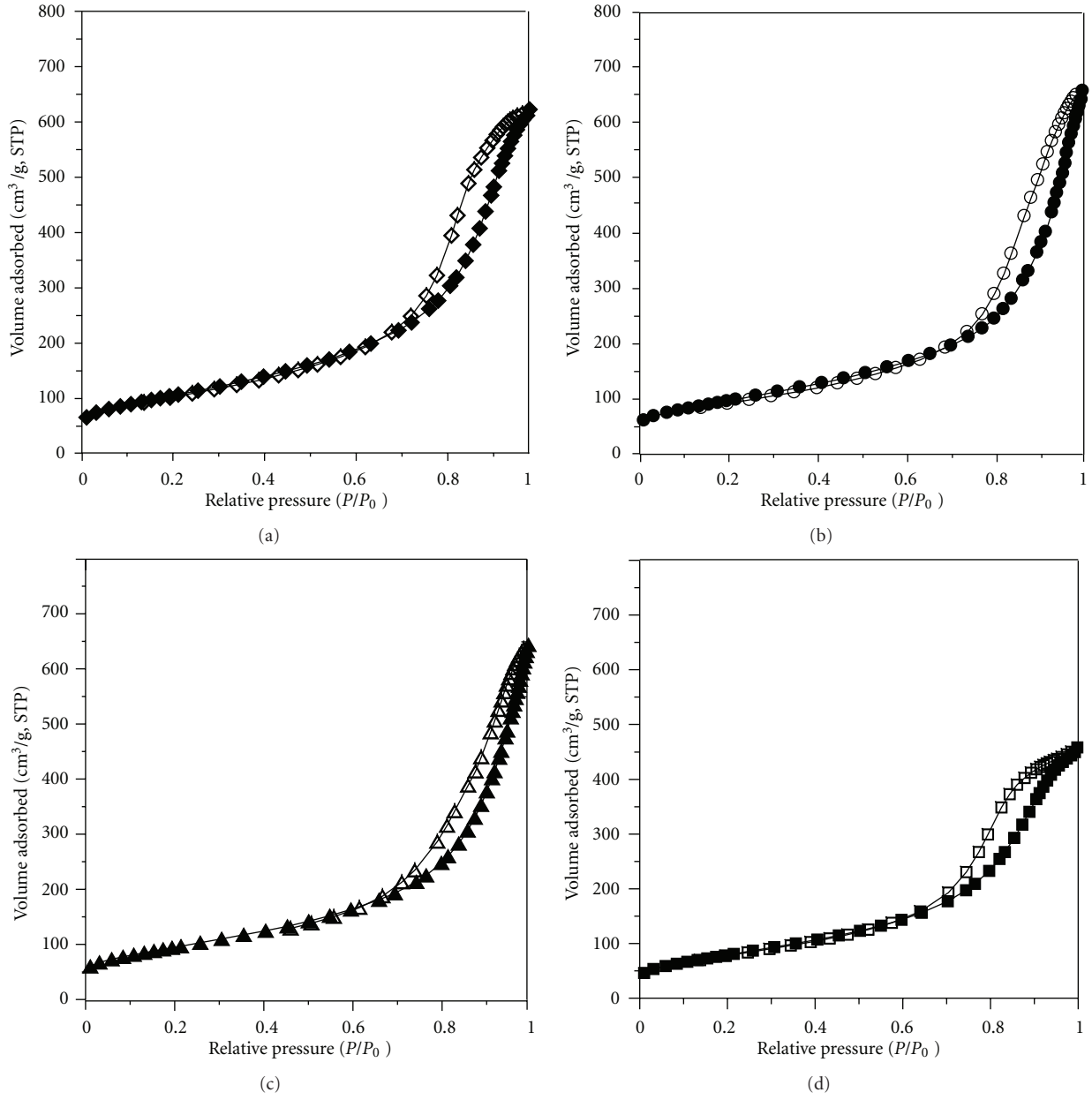

Figure 2: Adsorption (solid symbol)/desorption (empty symbol) isotherms of N_2 onto titania nanotubes at −196°C: (a) Co-1-TNT; (b) Co-3-TNT; (c) Co-5-TNT; (d) Co-7-TNT.

amounts of Co dopant are shown in Figure 4. It is known that the precursor P25 has *ca.* 70% anatase and *ca.* 30% rutile phases. It can be seen from XRD patterns that the representative peaks are anatase [101], [004], [200], [105], and [204] diffractions at scattering angles (2θ) of 25.3°, 36.6°, 48.0°, 55.0°, and 62.6°, respectively. It is obvious that the rutile of P25 has been transferred to anatase. The anatase phase with a longer *c* axis has been reported to be the preferred phase in TiO_2 nanotubes [7, 8]. Interestingly enough, the peak intensity is found to increase with the dopant concentration. Generally, the vague peaks reflect the small number of crystalline layers due to the small wall thickness of the tubes. This implies that the doping of Co may affect the rolling of the sheets; that is, different curvatures of rolled sheets would dominate the wall thickness of tubes.

The XRD cannot identify the low amount of Co dopant in titania nanotubes due to its detection limit. However, three diffraction peaks (101), (004), and (200) appear a slight shift after the introduction of Co dopant (see Figure 4), resulting in the small change of lattice parameters. Accordingly, this result reflects that the Co dapants insert into the crystalline TiO_2 structures without any Co or cobalt oxide coatings. The lattice parameters and interlayer distances of various titania nanotubes based on the XRD patterns are collected and listed in Table 2. It can be seen that undoped TiO_2 nanotubes have lattice parameters (*a*- and *c*-axis) of

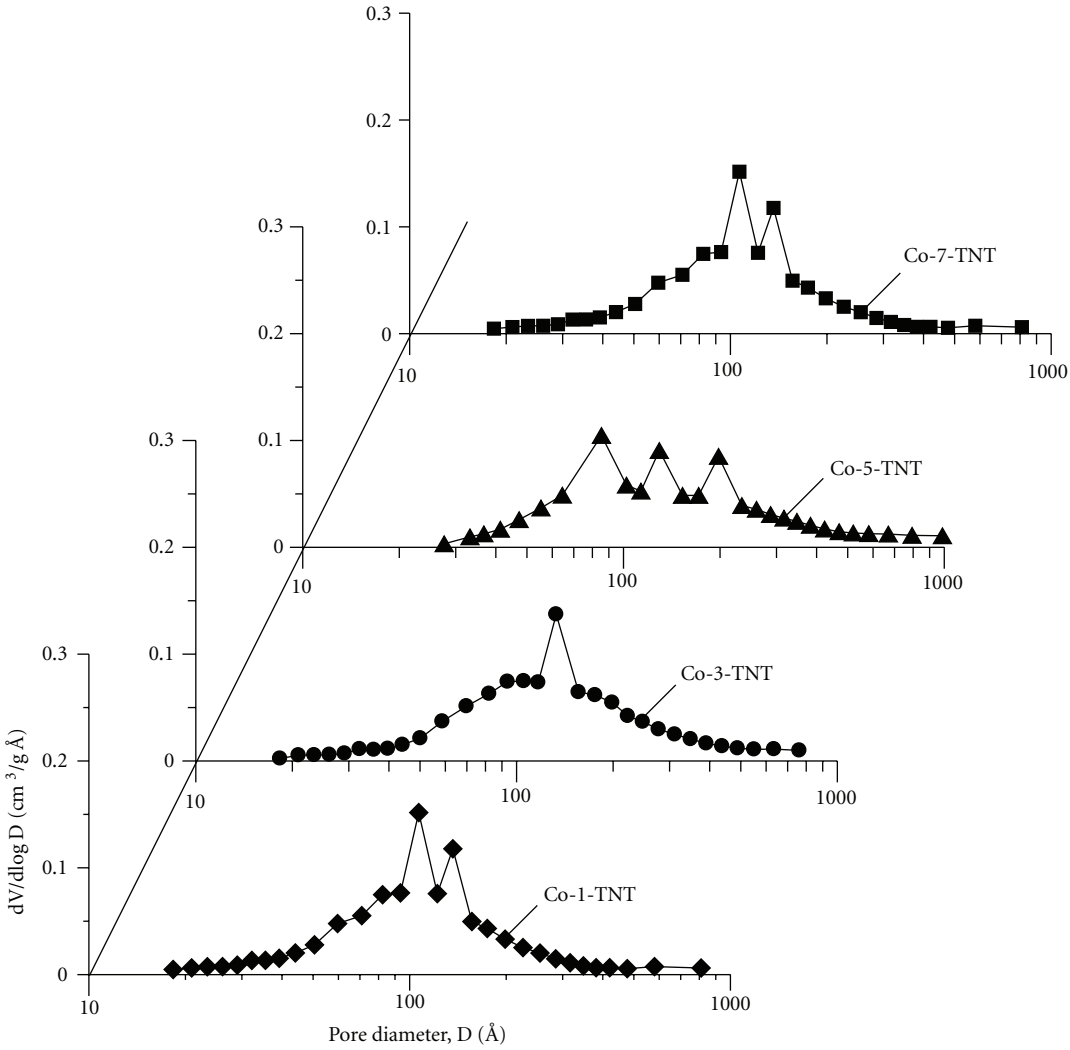

Figure 3: Pore size distributions of various Co-doped TiO_2 nanotubes determined from BJH method.

0.3710 and 0.9502 nm, respectively, in the unit cell based on the tetragonal Bravais lattice. In comparison with the Co-doped titania nanotubes, there exists derivations of 0.65%−2.05% (*a*-axis) and 0.44%−0.78% (*c*-axis), and the deviation increases with the amount of Co dopants. After the Co doping, the interlayer distances of $d_{(200)}$ and $d_{(004)}$ gradually extend, confirming the intercalation of Co dopants into the anatase-type crystals.

To inspect the concentration of Co dopant, an EDS technique was employed to measure atomic ratios of as-synthesized titania samples. Table 1 shows the atomic ratios of the nanotubes determined form EDS analysis. The weight percentage of Co dopant to TNT for all Co-doped titania nanotubes has an order as follows: Co-1-TNT (0.19%) < Co-3-TNT (0.43%) < Co-5-TNT (0.56%) < Co-7-TNT (0.73%). Generally, the atomic ratio of Co is found to be slightly lower than the operating ionic concentration in the precursor. The decrease can be attributed to the replacement of metal ions with protons during acid washing.

Figure 5 shows the diffuse reflection spectra of the titania nanotubes as a function of wavelength. It is well known

Table 2: Lattice parameters and interlayer distances of TiO_2 nanotubes with different amounts of Co dopants, based on the XRD patterns.

Materials	c (nm)	a (nm)	$d_{(200)}$ (nm)	$d_{(004)}$ (nm)
P25	0.9508	0.3708	0.1864	0.2377
TNT	0.9502	0.3710	0.1865	0.2380
Co-1-TNT	0.9544	0.3734	0.1867	0.2386
Co-3-TNT	0.9556	0.3748	0.1874	0.2389
Co-5-TNT	0.9568	0.3756	0.1878	0.2392
Co-7-TNT	0.9576	0.3786	0.1893	0.2394

that anatase-type TiO_2 crystalline structure has a strong absorption edge below *ca.* 380 nm [11]. The absorption edges of Co-doped TiO_2 nanotubes show a shift to visible-light region (i.e., >400 nm in wavelength). After that, an obvious peak is found within the wavelength region 550–650 nm, in where the peak height is found to increase with the dopant concentration. The absorption peak at 550–650 nm can be ascribed to the formation of impurity energy level

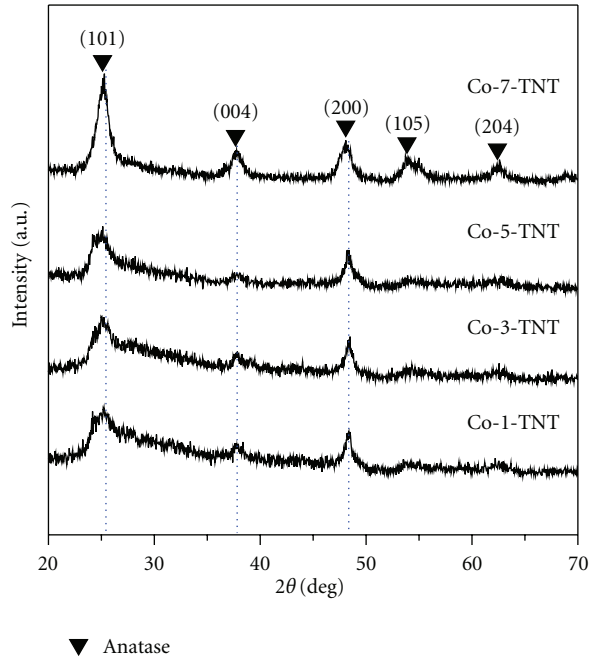

Figure 4: XRD patterns for Co-doped TiO_2 nanotubes prepared from hydrothermal treatment.

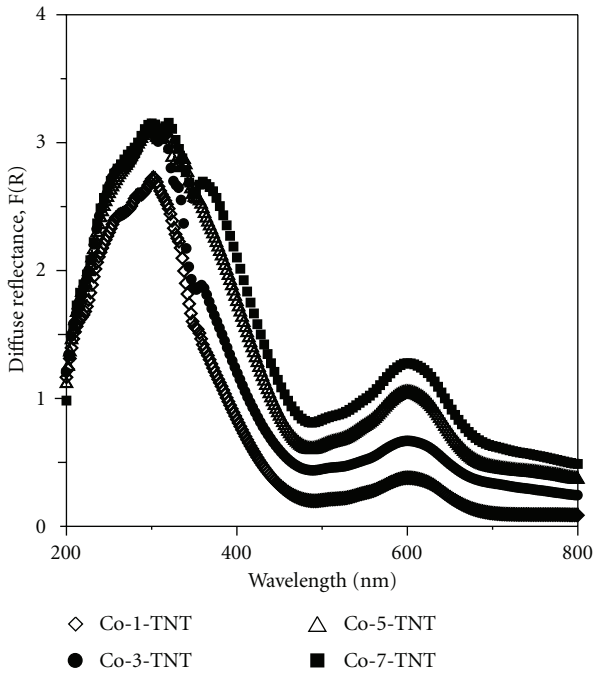

Figure 5: Diffuse reflection spectra for TiO_2 nanotubes with different Co dopant concentrations.

within the band gap. This proves that the hydrothermal doping technique has modified the UV-visible absorption characteristics of titania catalysts.

Theoretically, the absorption spectrum used for the calculation of band gap can be expressed in terms of $F(R)$, Kubelka-Munk (KM) model. The diffuse reflectance, R, of the titania sample is related to the KM function by [21–23]

$$F(R) = \frac{(1-R)^2}{2R} = \frac{\alpha}{S}, \quad (1)$$

where α and S represent the absorption coefficient and the scattering coefficient, respectively. The KM model is frequently used to estimate the absorption band gap based on the diffuse reflection spectra [21, 23]. The optical band energy of titania samples can be evaluated by using a linearity plot of $[F(R) \cdot h\nu]^{1/\eta}$ versus $h\nu$, in which $h\nu$ is the energy of the incident photon and the exponent η depends on the type of optical transition caused by photon absorption [23]. An excellent fitting was proposed by using the KM plots ($\eta = 2$) for the metal-oxide nanocrystals. As shown in Figure 6, the linearity KM plots were extended and intersected with x-axis, that is, the energy of the incident photon. The intersection represents the optical band gap of titania samples. It can be seen that all magnitudes of band gaps are smaller than 3.2 eV, and the optical band gap shows a decreasing trend with the Co dopant concentration: Co-1-TNT (2.3 eV) > Co-3-TNT (2.1 eV) > Co-5-TNT (2.0 eV) > Co-7-TNT (1.9 eV). The above results disclose two messages: (i) the Co dopants effectively make the band gap narrower and (ii) the variation of band gap depends on dopant concentration. Figure 7 shows a quantitative description of the band gap as a function of dopant concentration in Co-TiO_2 nanotubes. A gradual decreasing relationship between the optical band gap and the number of Co dopants confirms that the hydrothermal synthesis of Co doping in the TiO_2 nanotubes leads to a pathway of "communicated electrons" between these crystals.

3.3. Adsorption and Visible-Light Photocatalysis of MB on Co-TiO_2 Nanotubes. To examine the photocatalytic efficiency of titania samples, a possible mechanism for removing MB on Co-TiO_2 nanotubes is taken into account, which consists of (i) liquid-phase adsorption of MB and (ii) photocatalysis of adsorbed MB under fluorescent lamp. Numerous studies have proposed the similar photocatalytic mechanism in describing decomposition of various organics on TiO_2 and ZnO nanostructures [24–29]. Accordingly, the adsorption capability of MB on titania nanotubes plays an important role in affecting the photocatalytic efficiency. Thus, the active sites for MB adsorption are believed to be governed by the surface structure of titania nanotubes. To figure out adsorption and photocatalysis effects, an adsorption experiment in complete darkness is carried out first. The adsorption capacity as a function of time for all titania nanotubes is shown in Figure 8. An adsorption equilibrium of MB adsorption within 2 hr is reached, and the adsorption capacities show an order as follows: Co-1-TNT (110 mg/g) > TNT (101 mg/g) > Co-3-TNT (97 mg/g) > Co-5-TNT (91 mg/g) > Co-7-TNT (70 mg/g). These adsorption capacities of titania nanotubes are much higher than that of nanoparticles [30]. This order is generally followed by the magnitude of specific surface area of nanotubes, indicating

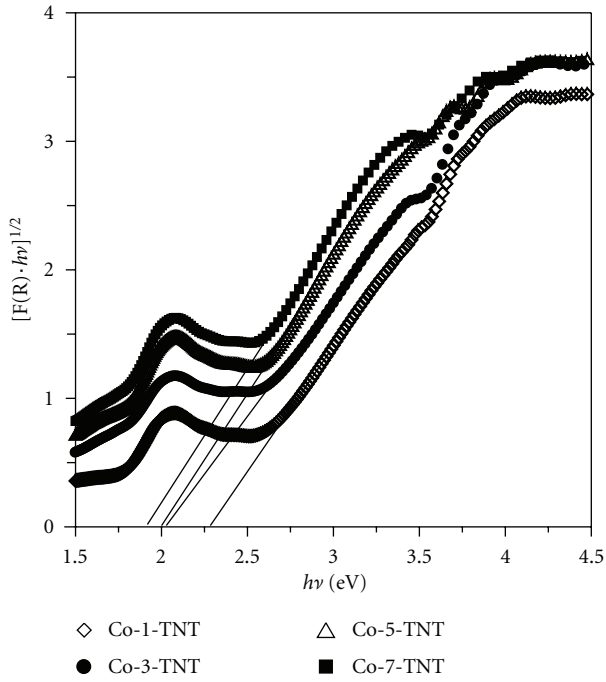

Figure 6: KM plots for TiO_2 nanotubes with different Co dopant concentrations.

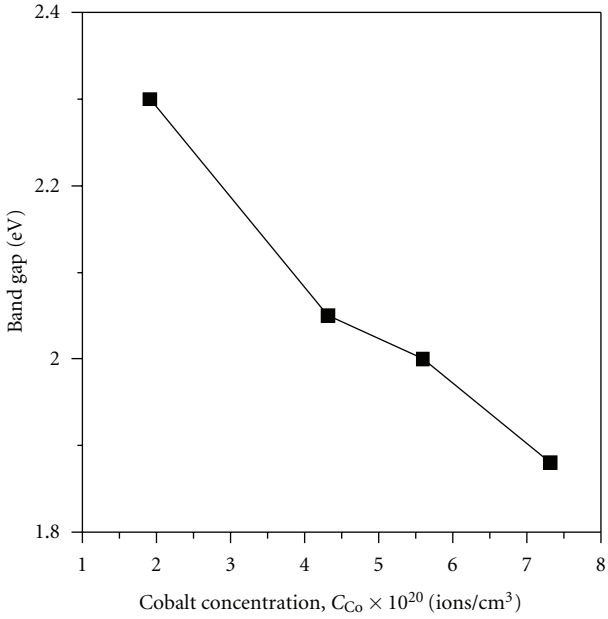

Figure 7: Variation of optical band gap with Co dopant concentration in TiO_2 nanotubes.

that the nanotubes offer different numbers of active sites for the MB adsorption in liquid phase.

As for MB-titania interaction, the electrostatic attraction plays a crucial role in the physical adsorption [31]. The adsorption process can be tentatively expressed in thermodynamic term as

$$\text{TNT}^* + \text{MB} \longleftrightarrow \text{TNT}^*(\text{MB}) \qquad \text{(R1)}$$

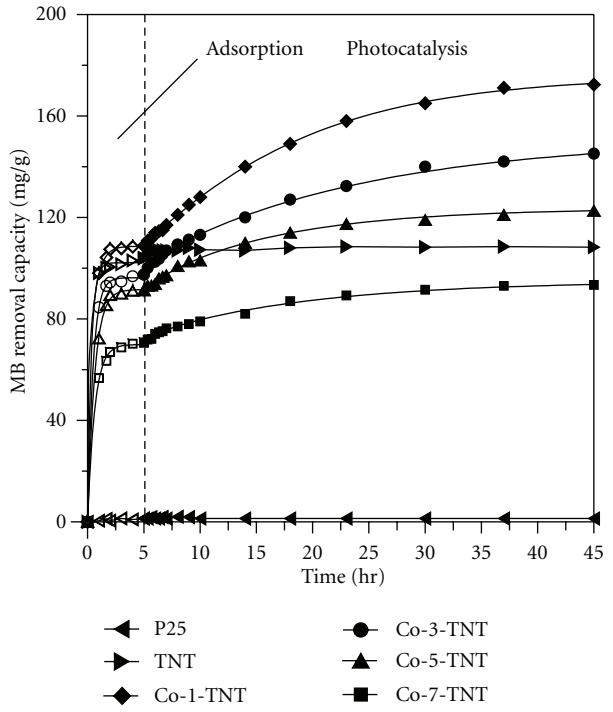

Figure 8: Liquid-phase adsorption of MB followed by visible-light photocatalysis kinetics of as-prepared product of Co-doped TiO_2 nanotubes at 40°C.

where MB represents the adsorbates in liquid phase, TNT* the available adsorptive sites on titania nanotubes, and TNT* (MB) the adsorptive sites occupied by MB molecules. The sum of TNT* and TNT* (MB) numbers is thus the total number of sites, capable of adsorbing the MB molecule at monolayer coverage (R1). The adsorptive surface coverage Θ_{ads}, that is, the fraction of BET area covered by MB molecules, can be evaluated by assuming that the area occupied by a MB molecule is estimated to be 130 Å^2 [31].

The calculated adsorptive coverage Θ_{ads} for the nanotubes ranges from 60% to 70%, proving the presence of surface heterogeneity for MB adsorption. The adsorptive coverage shed a clue that explores (i) the normalization of adsorptive areas due to different porosities of Co-doped TNTs and (ii) the number of active sites for adsorbing MB molecules from the initial aqueous solution. Since all Co-TiO_2 nanotubes has alike physically surface structure (e.g., mesopore fraction and pore size distribution), this difference among Θ_{ads} values is thus attributed to surface heterogeneity, contributed from the presence of Co dopants. Figure 9 shows the variation of surface coverage Θ_{ads} with Co dopant concentration. The adsorptive surface coverage (Θ_{ads}) smaller than 100% reflects that MB cannot completely wet titania surface in the adsorption system. Generally, the liquid-phase adsorption in the monolayer region is different from that in the multiplayer region, and the surface coverage possibly relates to hydrolyzed surface area and existence of –OH group over titania nanotubes. Basically, TiO_2 surface favors hydrophilic behavior [4], whereas metallic cobalt appears a more hydrophobic characteristic. Pan et al. have

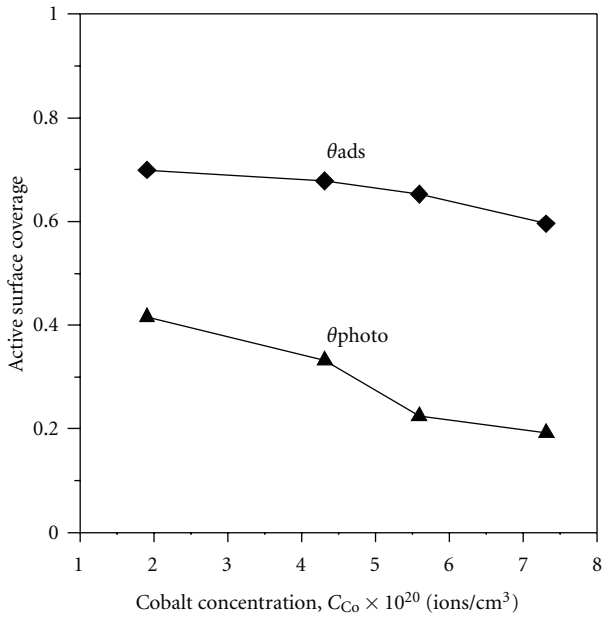

Figure 9: Variations of adsorptive surface coverage and photocatalyzed surface coverage with Co dopant concentration in TiO_2 nanotubes.

revealed the enhanced hydrophobicity of Co-doped TiO_2 nanocrystals [32]. However, it is worth noting that the MB molecules in aqueous solution are prone to be hydrates, favoring the surface of hydrophilic nanotubes. Accordingly, the adsorption capacity shows a gradual decreasing function of the amount of Co dopant. Thus, more Co doping would lead to the better water repellency, probably diminishing adsorptive surface coverage of MB in aqueous solution.

Visible-light photocatalysis of MB on Co-TiO_2 nanotubes is conducted after attaining adsorption saturation, and the photocatalytic kinetics are also shown in Figure 8. As expected, original TNT appears a little visible-light photocatalytic capability (<3 mg/g), whereas these Co-TiO_2 nanotubes display photocatalytic ability in decomposing organic dyes under fluorescent lamp. This proves that the hydrothermal synthesis of Co-TiO_2 tubes is an efficient approach in enhancing not only specific surface area but also photocatalysis performance under fluorescent lamp. Accordingly, the synergetic effect involves two key factors in affecting the photocatalytic activity of Co-doped titania nanotubes under fluorescent lamp, that is, high porosity and optical band gap. However, these kinetic curves appear a slower MB removal rate in comparison with the liquid-phase adsorption, since the photocatalytic equilibrium takes a long period of 40 hr. The visible-light photocatalytic effectiveness seems to be less significant than the adsorption.

The adsorption process has been illustrated as (R1). The photocatalysis of MB molecules under visible illumination can be considered as a surface-catalyzed reaction, which depends on the number of adsorptive sites and optical band gap of TS catalysts. It is generally recognized that conduction band electrons (e^-) and valence band holes (h^+) are generated on the surface of photocatalysts when the aqueous catalyst suspension is illuminated by light with an energy higher than the band gap energy [33], as expressed in (R2). Holes can react with water adhering to the surface of Co-TiO_2 nanotubes to form highly reactive hydroxyl radicals (OH•), as shown in (R3). Oxygen acts as an electron acceptor by forming a superoxide radical anion ($O_2^{\bullet -}$), as shown in (R4). The suspension of superoxide radical anions may act as oxidizing agents or as an additional source of hydroxyl radicals via the subsequent formation of hydrogen peroxide, as shown in (R5)–(R7). The strong oxidants associated with hydroxyl radicals react with adsorbed MB molecules, and make the blue solution colorless, as shown in (R8). Since decomposition reaction of the MB is composed of several steps, (R8) is just a simplified form [33].

$$TiO_2 + h\nu \longrightarrow e^- + h^+ \quad \text{(R2)}$$

$$H_2O + h^+ \longrightarrow OH\bullet + H^+ \quad \text{(R3)}$$

$$O_2 + e^- \longrightarrow O_2^{\bullet -} \quad \text{(R4)}$$

$$O_2^{\bullet -} + H^+ \longrightarrow HO_2\bullet \quad \text{(R5)}$$

$$2HO_2\bullet \longrightarrow H_2O_2 + O_2 \quad \text{(R6)}$$

$$H_2O_2 + O_2^{\bullet -} \longrightarrow OH\bullet + O_2 + OH^- \quad \text{(R7)}$$

$$OH\bullet + MB^+ \longrightarrow \text{colorless compound} \quad \text{(R8)}$$

Accordingly, this reaction (R2) enables the promotion of redox ability of the photogenerated electron-hole pairs, by carrying out the following sequences. The Co-doped crystals are capable of acquiring the excitation energy from visible irradiation. This is attributed to the fact that its narrow band gap easily obtains the electron-hole pairs over the nanotubes under fluorescent lamp, thus, leading to the photocatalytic activity.

The photocatalytic reaction is basically a surface reaction that is assumed to take place on the adsorptive site. If this assumption is correct, the surface coverage of photocatalysis sites should be the same as that of adsorptive sites based on equal apparent rate constants. According to the photocatalytic capacity at 40 hr visible illumination, the surface coverage for MB photocatalysis (Θ_{photo}) is evaluated for proving the above assumption. The relation of calculated Θ_{photo} values versus Co dopant concentration is also plotted in Figure 9. It can be seen that the two surface coverages, Θ_{ads} and Θ_{photo}, cannot match each other, indicating that the assumption fails. The smaller value of Θ_{photo} (i.e., within 20%–40%) shows that only 50%–60% MB-adsorbed sites would be photocatalyzed under fluorescent lamp. This result can be attributed to two possible explanations. The first one is that the source of visible-light irradiation in this study is too weak to photogenerate enough number of electron/hole pairs, thus partially photocatalyze some MB-adsorbed sites. Secondly, the photocatalysis is a parallel and complicated chemical reaction (R2)–(R8), showing a higher energy barrier than the physical adsorption needed. Generally, the physical adsorption of MB would take place on nonspecific sites, whereas the photocatalysis generates

only on some specific adsorptive sites. On specific sites, the photoexcited energy required (1.8–2.4 eV) is one or two order higher than the physisorption. Additionally, the visible photocatalysis of MB takes a very long period in comparable to the physisorption, as shown in Figure 8. This means that the serial of photocatalytic reactions (R2)–(R8), including photoinduction, electron/hole generation, radical formation, and MB decomposition, thus become a rate-determining step during MB decomposition process. Thus, this may induce a lower surface coverage for photocatalysis of MB under fluorescent lamp.

As shown in Figure 9, the value of Θ_{photo}, is also a decreasing function of the Co dopant concentration. Again, this confirms that the optical band gap is not the key factor in affecting the visible photocatalytic performance. In this work, 1 at. % Co dopant concentration in titania crystalline structure is competence for visible photocatalysis. This couple of decline relationship in Figure 9 can be ascribed to that total amount of adsorptive sites significantly affects the number of photocatalyzed sites. Accordingly, titania nanotubes with a large number of pores are expected to facilitate the liquid-phase adsorption capacity, which also induces the enhancement of the visible photocatalysis capability.

4. Conclusions

The present work showed efficient Co doping of highly porous TiO_2 nanotubes by hydrothermal synthesis. The specific surface areas of Co-doped TiO_2 nanotubes were found to have a great value of *ca.* 289–379 m^2/g. These tubes were shown to be hollow scrolls with a typical outer diameter of about 10–15 nm, inner diameter 5–10 nm and length of several micrometers. The titania nanotubes had an anatase-type crystalline structure. UV absorption analysis reflected that these titania nanotubes show a strong absorption in the visible range and narrow optical band gap within 1.8–2.4 eV, according to the KM plots. We have confirmed that the Co-TiO_2 nanotubes displayed a photocatalysis ability in decomposing organic dyes under fluorescent lamp. The visible photocatalysis would take a long period of 40 hr, indicating that the visible photocatalysis is a rate-determining step during the MB removal process. On the basis of the results, the hydrothermal synthesis of Co-TiO_2 tubes is an efficient approach in enhancing not only specific surface area, but also photocatalysis capability under fluorescent lamp. This novel titania nanostructure, Co-doped titania nanotubes, can improve the photocatalytic efficiency in a variety of photocatalysis applications because of the combination effect of a high porosity with a visible-light-derived photocatalysis.

Acknowledgment

The authors are very grateful for the financial support from the National Science Council of the Republic of China under the contracts NSC 100-2120-M-155-031, NSC 100-2221-E-155-078, and NSC 99-2632-E-155-001-MY3.

References

[1] A. Ghicov, J. M. Macak, H. Tsuchiya et al., "Ion implantation and annealing for an efficient N-doping of TiO_2 nanotubes," *Nano Letters*, vol. 6, no. 5, pp. 1080–1082, 2006.

[2] C. C. Tsai and H. Teng, "Regulation of the physical characteristics of titania nanotube aggregates synthesized from hydrothermal treatment," *Chemistry of Materials*, vol. 16, no. 22, pp. 4352–4358, 2004.

[3] G. K. Mor, K. Shankar, M. Paulose, O. K. Varghese, and C. A. Grimes, "Enhanced photocleavage of water using titania nanotube arrays," *Nano Letters*, vol. 5, no. 1, pp. 191–195, 2005.

[4] L. Qian, Z. S. Jin, S. Y. Yang, Z. L. Du, and X. R. Xu, "Bright visible photoluminescence from nanotube titania grown by soft chemical process," *Chemistry of Materials*, vol. 17, no. 21, pp. 5334–5338, 2005.

[5] P. Umek, P. Cevc, A. Jesih, A. Gloter, C. P. Ewels, and D. Arčon, "Impact of structure and morphology on gas adsorption of titanate-based nanotubes and nanoribbons," *Chemistry of Materials*, vol. 17, no. 24, pp. 5945–5950, 2005.

[6] H. Kim, R. C. Y. Auyeung, M. Ollinger, G. P. Kushto, Z. H. Kafafi, and A. Piqué, "Laser-sintered mesoporous TiO_2 electrodes for dye-sensitized solar cells," *Applied Physics A*, vol. 83, no. 1, pp. 73–76, 2006.

[7] C. C. Tsai and H. Teng, "Structural features of nanotubes synthesized from NaOH treatment on TiO_2 with different post-treatments," *Chemistry of Materials*, vol. 18, no. 2, pp. 367–373, 2006.

[8] B. D. Yao, Y. F. Chan, X. Y. Zhang, W. F. Zhang, Z. Y. Yang, and N. Wang, "Formation Mechanism of TiO_2 Nanotubes," *Applied Physics Letters*, vol. 82, p. 281, 2003.

[9] J. N. Nian and H. Teng, "Hydrothermal synthesis of single-crystalline anatase TiO_2 nanorods with nanotubes as the precursor," *Journal of Physical Chemistry B*, vol. 110, no. 9, pp. 4193–4198, 2006.

[10] S. Nakade, Y. Saito, W. Kubo, T. Kitamura, Y. Wada, and S. Yanagida, "Influence of TiO_2 nanoparticle size on electron diffusion and recombination in dye-sensitized TiO_2 solar cells," *Journal of Physical Chemistry B*, vol. 107, no. 33, pp. 8607–8611, 2003.

[11] M. Anpo, "Use of visible light. Second-generation titanium oxide photocatalysts prepared by the application of an advanced metal ion-implantation method," *Pure and Applied Chemistry*, vol. 72, no. 9, pp. 1787–1792, 2000.

[12] M. Harada, T. Sasaki, Y. Ebina, and M. Watanabe, "Preparation and characterizations of Fe- or Ni-substituted titania nanosheets as photocatalysts," *Journal of Photochemistry and Photobiology A*, vol. 148, no. 1-3, pp. 273–276, 2002.

[13] M. Anpo and M. Takeuchi, "The design and development of highly reactive titanium oxide photocatalysts operating under visible light irradiation," *Journal of Catalysis*, vol. 216, no. 1-2, pp. 505–516, 2003.

[14] D. Dvoranová, V. Brezová, M. Mazúr, and M. A. Malati, "Investigations of metal-doped titanium dioxide photocatalysts," *Applied Catalysis B*, vol. 37, no. 2, pp. 91–105, 2002.

[15] R. Asahi, T. Morikawa, T. Ohwaki, K. Aoki, and Y. Taga, "Visible-light photocatalysis in nitrogen-doped titanium oxides," *Science*, vol. 293, no. 5528, pp. 269–271, 2001.

[16] D. Li and H. Haneda, "Synthesis of nitrogen-containing ZnO powders by spray pyrolysis and their visible-light photocatalysis in gas-phase acetaldehyde decomposition," *Journal of Photochemistry and Photobiology A*, vol. 155, no. 1-3, pp. 171–178, 2003.

[17] M. Jansen and H. P. Letschert, "Inorganic yellow-red pigments without toxic metals," *Nature*, vol. 404, no. 6781, pp. 980–982, 2000.

[18] P. G. Wu, C. H. Ma, and J. K. Shang, "Effects of nitrogen doping on optical properties of TiO_2 thin films," *Applied Physics A*, vol. 81, no. 7, pp. 1411–1417, 2005.

[19] C. T. Hsieh, W. S. Fan, W. Y. Chen, and J. Y. Lin, "Adsorption and visible-light-derived photocatalytic kinetics of organic dye on Co-doped titania nanotubes prepared by hydrothermal synthesis," *Separation and Purification Technology*, vol. 67, no. 3, pp. 312–318, 2009.

[20] D. Wu, Di, Y. Chen et al., "Co-doped titanate nanotubes," *Applied Physics Letters*, vol. 87, no. 11, pp. 112501–112501-3, 2005.

[21] E. S. Brigham, C. S. Weisbecker, W. E. Rudzinski, and T. E. Mallouk, "Stabilization of intrazeolitic cadmium telluride nanoclusters by ion exchange," *Chemistry of Materials*, vol. 8, no. 8, pp. 2121–2127, 1996.

[22] M. D. Argyle, K. Chen, C. Resini, C. Krebs, A. T. Bell, and E. Iglesia, "Extent of reduction of vanadium oxides during catalytic oxidation of alkanes measured by in-situ UV-visible spectroscopy," *Journal of Physical Chemistry B*, vol. 108, no. 7, pp. 2345–2353, 2004.

[23] D. G. Barton, M. Shtein, R. D. Wilson, S. L. Soled, and E. Iglesia, "Structure and electronic properties of solid acids based on tungsten oxide nanostructures," *Journal of Physical Chemistry B*, vol. 103, no. 4, pp. 630–640, 1999.

[24] J. Matos, J. Laine, and J. M. Herrmann, "Effect of the type of activated carbons on the photocatalytic degradation of aqueous organic pollutants by UV-irradiated titania," *Journal of Catalysis*, vol. 200, no. 1, pp. 10–20, 2001.

[25] J. Matos, J. Laine, and J. M. Herrmann, "Synergy effect in the photocatalytic degradation of phenol on a suspended mixture of titania and activated carbon," *Applied Catalysis B*, vol. 18, no. 3-4, pp. 281–291, 1998.

[26] L. Zou, Y. Luo, M. Hooper, and E. Hu, "Removal of VOCs by photocatalysis process using adsorption enhanced TiO_2-SiO_2 catalyst," *Chemical Engineering and Processing*, vol. 45, no. 11, pp. 959–964, 2006.

[27] S. Kaneco, H. Katsumata, T. Suzuki, and K. Ohta, "Titanium dioxide mediated photocatalytic degradation of dibutyl phthalate in aqueous solution-kinetics, mineralization and reaction mechanism," *Chemical Engineering Journal*, vol. 125, no. 1, pp. 59–66, 2006.

[28] Y. Yu, J. C. Yu, C. Y. Chan et al., "Enhancement of adsorption and photocatalytic activity of TiO_2 by using carbon nanotubes for the treatment of azo dye," *Applied Catalysis B*, vol. 61, p. 1, 2005.

[29] Y. Yu, J. C. Yu, J. G. Yu et al., "Enhancement of photocatalytic activity of mesoporous TiO_2 by using carbon nanotubes," *Applied Catalysis A*, vol. 289, p. 186, 2005.

[30] M. L. Fetterolf, H. V. Patel, and J. M. Jennings, "Adsorption of methylene blue and acid blue 40 on titania from aqueous solution," *Journal of Chemical and Engineering Data*, vol. 48, no. 4, pp. 831–835, 2003.

[31] Y. R. Lin and H. Teng, "Mesoporous carbons from waste tire char and their application in wastewater discoloration," *Microporous and Mesoporous Materials*, vol. 54, no. 1-2, pp. 167–174, 2002.

[32] D. Pan, G. Xu, J. Wan, Z. Shi, M. Han, and G. Wang, "Tuning the solubility of TiO_2 Nanoparticles in apolar solvents by doping with Co2+," *Langmuir*, vol. 22, no. 13, pp. 5537–5540, 2006.

[33] H. F. Lin, S. C. Liao, and S. W. Hung, "The dc thermal plasma synthesis of ZnO nanoparticles for visible-light photocatalyst," *Journal of Photochemistry and Photobiology A*, vol. 174, no. 1, pp. 82–87, 2005.